Near-Ballistic Transport in Single-Ferrocene Junctions with Multiple Contact Points

Albert C. Aragonès,[†ν] Nadim Darwish,[#] Simone Ciampi,[#] Li Jiang,[‡] Raphael Roesch,[|] Eliseo Ruiz,[*^ν] Christian A. Nijhuis[*‡Δ] and Ismael Díez-Pérez [*†§ν]

[†] Department of Chemistry, Faculty of Natural & Mathematical Sciences, King's College London, Britannia House, 7 Trinity Street, London SE1 1DB, United Kingdom.

[ν] Institut de Química Teòrica i Computacional (IQTC), Universitat de Barcelona, Diagonal 645, 08028 Barcelona.

[^] Departament de Química Inorgànica i Orgànica, Universitat de Barcelona, Diagonal 645, 08028 Barcelona, Spain.

[§] Centro Investigación Biomédica en Red (CIBER-BBN). Campus Río Ebro-Edificio I+D, Poeta Mariano Esquillor s/n, 50018 Zaragoza, Spain.

[#] Department of Chemistry, Curtin University, Bentley WA 6102, Australia.BF

[‡] Department of Chemistry, National University of Singapore, 3 Science Drive 3, Singapore 117543.

[Δ] Centre for Advanced 2D Materials, National University of Singapore, 6 Science Drive 2, Singapore 117546.

[|] Center for Biosensors and Bioelectronics, Biodesign Institute, Arizona State University, Tempe, Arizona 85287, USA.

TOC

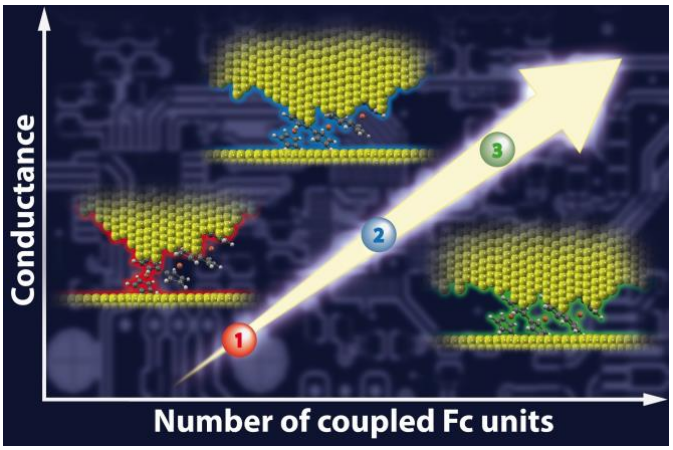

Abstract:

Ferrocene (Fc) is a promising candidate for nanoscale molecular devices since it offers electronic functions due to its low-lying highest occupied molecular orbital and high chemical stability. This paper reports highly efficient coherent tunneling in single-molecule wires of oligo-ferrocenes with one to three Fc units. The Fc units were directly coupled to the electrodes, *i.e.* without chemical anchoring groups between the Fc units and the terminal electrodes. We found that a single Fc unit readily interacts with the metal electrodes of an STM-break junction (STM = scanning tunneling microscope) and that the zero voltage bias conductance of an individual Fc molecular junction increased 5-fold, up to 80% of the conductance quantum G_o (77.4 μS), when the length of the molecular wire was increased from one to three connected Fc units. Our compendium of experimental evidences combined with non-equilibrium Green functions calculations contemplate a plausible scenario to explain the exceedingly high measured conductance based on the electrode/molecule contact via multiple Fc units. The oligo-Fc backbone is initially connected through all present Fc units and, as the molecular junction is pulled away, each Fc unit is sequentially disconnected from one of the junction terminals resulting in a number of distinct conductance features proportional to the number of Fc units in the backbone. The conductance values are independent of the applied temperature (-10 to 85°C), which indicates that the mechanism of charge transport is coherent tunneling for all measured configurations. The measured conductance decrease agrees nicely with our transmission calculations and it is interpreted as the subtle decrease of the electrode/molecule coupling constant (effective number of e-pathways, linked to QI?) as a function of the molecular junction pulling distance. These measurements show the direct Fc-electrode coupling provides highly efficient molecular conduits with very low barrier for electron tunneling, and whose conductivity can be modulated near the ballistic regime.

Introduction

Molecular electronics consolidates as a research field that aims to complement traditional silicon integrated micro-circuits with molecular circuitry based on single molecules or self-assembled monolayers (SAMs).[1,2] Realizing molecular circuitries requires understanding the mechanisms of charge transport through metal-molecule-metal junctions, both experimentally and theoretically. Significant advances have been made towards understanding the fundamentals of single-molecules and SAMs charge transport in a very broad variety of molecular systems, reproducing a number of conventional electrical effects in molecular devices such as resistance,[3] transistor or diode effects,[4–8] in addition to fundamental studies of mechanisms of charge transport as a function of molecular length,[9–12] conjugation,[13–16] chemical substitutuents,[17–19] molecular conformation,[13,20–22] alignment of the molecular frontier orbitals to the electrode Fermi energy level,[23–26] aromaticity,[23,27] or anchoring group.[28–31] Most of these examples show conductance values of typically several orders of magnitudes below the conductance quantum G_0=77.4 µS, which evidences their resistive nature and their limitation as electron conduits in a molecular circuit.

Ferrocene (Fc) was the first example of a metallocene and it has been attractive in molecular electronics because of its good thermal and chemical stability and low-lying highest occupied molecular orbital (HOMO).[32–34] Fc binds weakly to the surface of common metals substrates such as Ag, Cu, Al, Mo or Au.[33,35–40] The Fc physisorbed on flat metal surfaces such as Ag (100), Cu (111) and Au (111) binds with the plane of the cyclopentadienyl moieties facing the surface.[33,36,41,42] These properties make Fc an attractive candidate in molecular electronics to provide simple electronic functions when properly linked to an electronic platform, including low resistivity and sharp gate-dependence,[43–46] or more complex operations such as negative differential resistance,[43,47] rectification[6,7,34,48] or Boolean logics.[7] A key parameter to achieve such large electrical tunability is the control over the Fc-electrode electronic coupling. Some applications require a weak Fc-electrode coupling to minimize the hybridization of the low-lying molecular orbital (here a HOMO), directly involved in the molecular charge transport, to the electrodes terminal[6,48]. Contrarily, a "high coupling" scenario could be designed by manipulating the delocalization of the low-lying HOMO level between several Fc units within the same molecular wire,[49,50] which, in turn, hybridizes to the device electrodes.[6,34] The latter is a much less studied case scenario that could be exploited to build efficient molecular wires displaying high conductance G values close to G_0.[44,51]

Here, we present a study of room-temperature single-molecule transport in STM break junctions of a new class of molecular wires composed of oligo-ferrocenes with one, two, and three directly connected ferrocene units, namely ferrocene (Fc), biferrocene (BFc) and 1-1'-terferrocene (TFc) (Fig. 1). The Fc units strongly interact with the terminal electrodes because of the high reactivity of uncoordinated gold atoms of the STM junction, without the need for additional anchoring groups such as thiolates or amines. We show that each individual Fc moiety can readily form highly conducting single-molecule junctions facilitating multiple Fc-electrode contacts with well-defined conductance signatures. Our single-molecule transport results show that the average number of conductance values (peaks) in a conductance histograms is equal to the number of ferrocene units present in the studied molecular backbone. These data suggest that each Fc unit is able of independently bridging the two electrodes terminals opening parallel electron pathways (greatly increasing the electron transmission) without the need for commonly used anchoring chemistry such as thiols or amines.[28,31] This new conformation in a single-molecule

junction can be used to interpret unexpectedly high G features observed in previous measurements incorporating Fc units.[44,46] Moreover, as opposed to previous single-molecule results in different oligomeric backbones with multi-anchoring points,[14,52,53] we observed that the conductance for each oligo-ferrocene conformation is "tuned" by the number and proximity of all connected ferrocene units connected to it (QI clear in next section?). The values of all measured set of conductances (G) are independent of the temperature suggesting that coherent tunneling is the dominant mechanism of charge transport across the ferrocene-based wires. The observed G decay between the different proposed contact configurations in the BFc and TFc can be pictured as a decrease in the molecule/electrode coupling constant to one of the electrodes as the junction is being pulled away and the number of effective Fc/electrodes connections is sequentially decreased. The computed DFT frontier orbitals and the transmission probability functions throughout all Fc-oligomers show an extended π-frontier orbitals delocalization along the molecular wire and a single-molecule transport dominated by the tail of the HOMO transmission peak, respectively. These results suggest Fc-oligomers as a new class of efficient nanoscale molecular wires with near ballistic transport and it also demonstrates the use of Fc as a new tunable molecule/electrode anchoring group with multiple contact points (through each individual Fc unit).

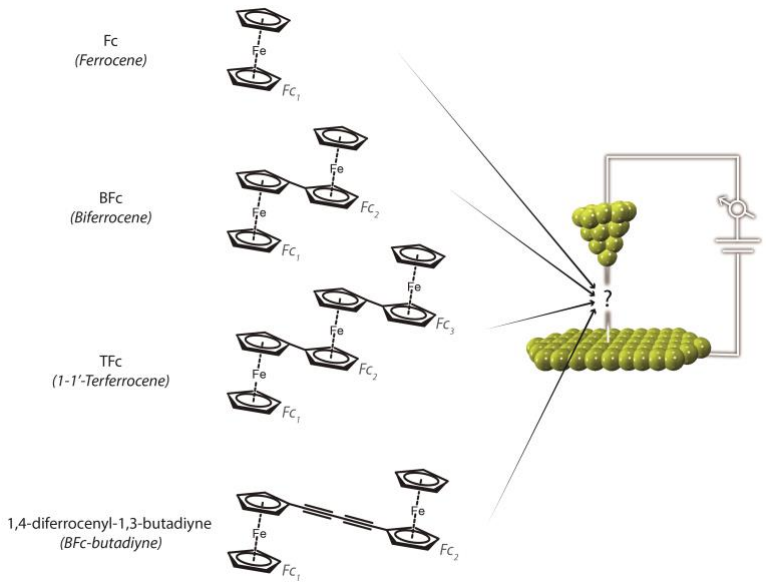

Fig. 1 Molecular structures of all studied oligo-ferrocenes in this work. The individual ferrocene units are labeled as Fc_1, Fc_2 and Fc_3. In the text, we abbreviate ferrocene as Fc, biferrocene as BFc, terferrocene as TFc and 1,4-diferrocenyl-1,3-butadiyne as BFc-butadiyne. Al, can u remove Fc_n labels ? , we don't need them anymore in the new notation)

Results and discussion

The single-molecule junctions

We measured the single-molecule conductance within a high conductance range near G_o (10^{-2} G_0 to $1G_0$) for the Fc, BFc, TFc and BFc-butadyine molecules (see details of the synthesis in the Supporting Information (SI) section 1) using the STM Break-junction (STM-BJ) technique.

Technical details of the STM-BJ approach have been published elsewhere[3,23] (for more details see SI section 2). Briefly, a STM Au tip is firstly brought over a flat, clean Au(111) surface to a tunneling distance in a solution containing the molecule of interest. Then, the STM current feedback is turned off and the STM tip is repeatedly driven in and out of contact to the Au(111) surface. During the retraction stage, individual molecules that are either dissolved in the surrounding organic medium or adsorbed on the surface can spontaneous bridge between the two electrodes. This pulling process is repeated thousands of times while the current is monitored, resulting in the collection of large amounts of current decay curves (4000–5000, see representative examples in Fig. 2 insets). Of these curves, 15-20% display plateau features corresponding to the quantum conductance of the single-molecule bridge.[54–56] Because not every current decay curve shows such plateau features, we designed an automatic algorithm that identifies and selects curves containing such single-molecule features. The exact same selection criteria were applied throughout all measured series (see more details in SI section 2). Conductance histograms were built by the accumulation of hundreds of selected individual current decays (displaying plateaus) and the resulting peak maxima represent the most probable conductance values of the studied single-molecule bridge. 1,2,4-Trichlorobenzene was employed as the solvent in all transport experiments (see SI sections 3 for more details and control experiments with different solvents).[57] It is worth noting from Figure 2 that each Fc unit establishes a well-defined contact geometry characterized by a single, symmetrical conductance signature (peak) as opposed to previously widely used anchoring chemistry that often result in multiple peaks, or shoulders and/or tails.[58–61]

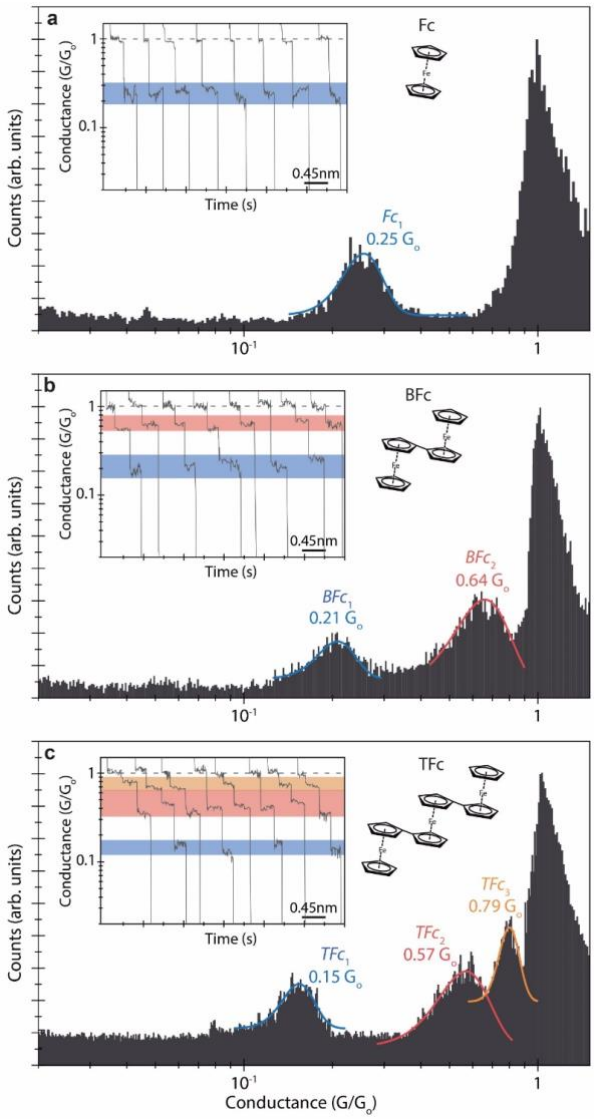

Fig. 2 Semi-log conductance histograms of the Fc **(a)**, BFc **(b)** and TFc **(c)** oligomers. Individual Gaussian fits of the peaks are used to extract the maxima values (indicated in the plot). The different molecular wire configurations are labeled as "$(oligoFc)_n$", being n the number of effectively bridged Fc units and the "oligo" term refereeing to Bi (B) or Ter (T). The insets show representative individual current traces displaying plateau features used to build the 1D histograms (2D maps accumulating all individual traces are shown in the SI section 4). Shadow colored lines are a visual guidance of the range of conductance for each configuration. Counts have been normalized versus the total amount of counts. The applied voltage bias was set to 10 mV.

Sequentially disconnecting Fc units

Figures 2a-c show a good correlation between the observed number of peaks within the studied high conductance range and the number of Fc units of the studied Fc-oligomer compound. A single plateau is always observed in the individual current decays for junctions with Fc (Fig. 2a), whereas junctions with BFc and TFc (Fig. 2b-c insets) shows that as the molecular junction is stretched (the Au STM tip electrode is pulled away from the Au surface), multiple plateaus concatenate with a good correlation in number to the number of existing Fc units in the backbone (Fig. 2a-c insets).[62,63] To analyze this correlation in detail, we plotted the data in a 2D

cross-correlation conductance map (see SI section 2 for additional details). Figure 3a shows the map for the molecular junction formed with the TFc,[64,65] which is represented by a 2D histogram of the analyzed counts at a particular conductance value of the individual decay curve (Y-axis) against the full measured conductance range (X-axis). The appearance of the three red spots along both X and Y directions at the conductance values coincidental with the three conductance maxima (Fig. 2c) evidences statistical correlation between the occurrences of the three plateaus. Given the observed high G values of such single-molecule junctions (reaching $0.8G_o$ in the TFc case) and their sequential nature, we hypothesize that the molecular junction forms effective parallel electron pathways by bridging multiple Fc units at the same time (Fig. 3b). This particular bridging configuration for BFc and TFc will be denoted by BFc_n and TFc_n, where *n* defines the number of Fc units effectively connected between the two electrodes (Fig. 3b). Figure 3a shows that the formation of the three molecular junction configurations, namely TFc_3, TFc_2 and TFc_1, occurs statistically in a sequential fashion as the tip retracts while sequentially unplugging each of the three Fc units (Fig. 3b).[53,63,66] With this picture in mind, Figure 3c summarizes the different conductance trends and hypothesized molecular junction configurations that will be challenged in the last section by computational calculations.

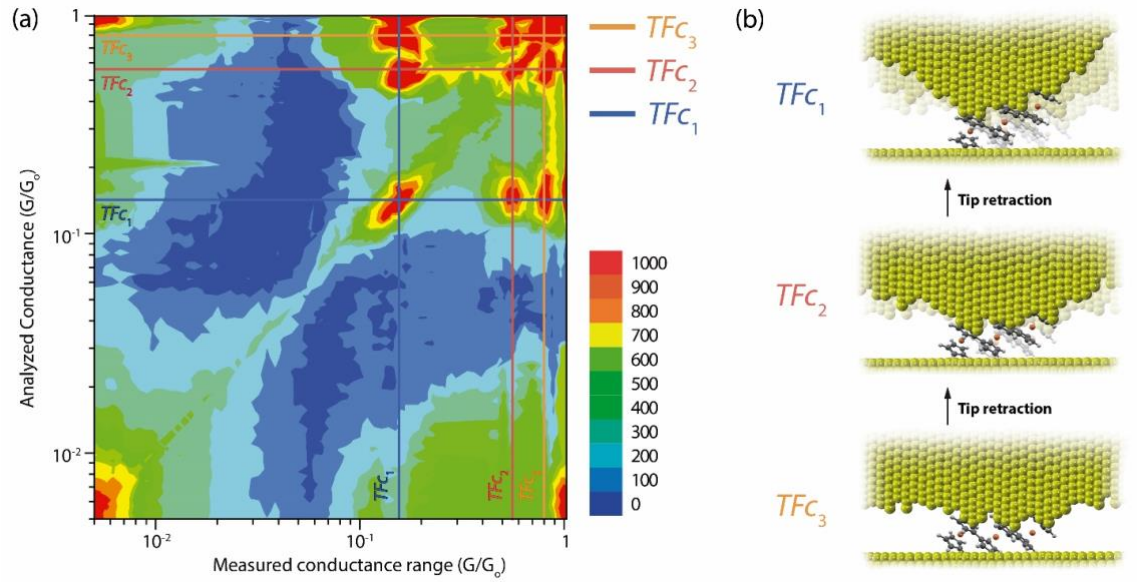

Fig. 3 (a) Logarithmic 2D cross-correlation conductance map of the individual traces for the TFc system. The horizontal lines are the selected conductance bins that registered higher counting coming from the three measured conductance plateaus of the TFc_3, TFc_2 and TFc_1 contact configurations (see Fig. 2 for notation). The vertical lines correspond to the measured conductance peaks showing up in the Fig. 2c histogram. The high-counts spots appearing at the intercrossing of all lines for each molecular wire configuration evidences the high sequential correlation of the three conductance events. The diagonal line reproduces the 1D conductance histograms of Fig. 2c. The high-counts spots labeled with an asterisk and a cross signs correspond to the background and saturation lines respectively, which are equally well correlated at the opposite corners of the map. **(b)** Cartoon representing the pulling sequence of a TFc molecular junction. As the STM tip is retracted, the initially bridged Fc units are sequentially disconnected from one of the electrodes terminal. **(c)** Posem aki la Fig. 8a resum. Al , check els valors de conductancies al teu graph resum, el TFc2 esta malament?!. Cambia els labels: G vs length, G vs Fc connected units, G vs backscattering.

Temperature independent single-molecule conductance

To determine the mechanism of charge transport through the Fc-based single-molecule wires, we measured their single-molecule conductance as a function of temperature *T*. Single-molecule transport experiments for Fc, BFc_1 and TFc_1 configurations with lower electrode-Fc connections were performed for varying *T*s from -10°C to 85°C (see also SI section 6). The Arrhenius plots (Fig. 4) of the averaged conductance values (*G* mean) show no significant dependence on *T* in all cases, indicating that the mechanism of charge transport is off-resonant tunneling for all wire contact configurations.[9,10]

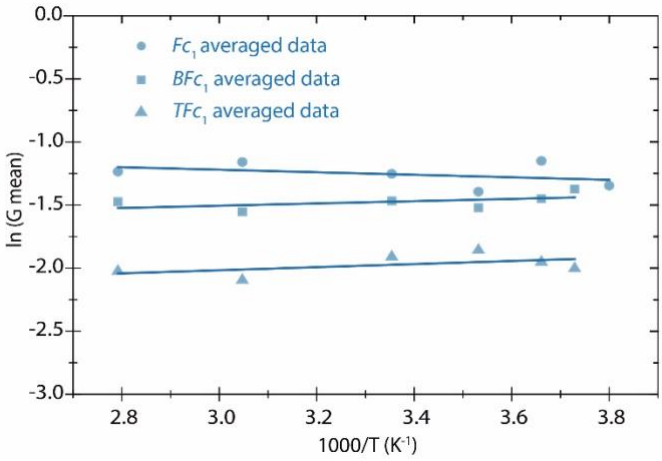

Fig. 4 Arrhenius plot of the Fc, BFc_1 and TFc_1 wires configurations, representing the log of the average single-molecule conductance (G mean) versus the inverse of temperature. The applied voltage bias was set to 10 mV.

Tuning the Fc-Fc electronic coupling (or supporting the multi-pathways structure)

We can fine-tune the high conductance values of the oligo-ferrocene wires by engineering the extension of the electronic coupling between the nearest Fc neighbors units, which, in turn, modulates the energy of the frontier orbital (see next computational section) and so the molecular device conductance. As a probe of this concept, we synthesized a diferrocenyl compound, 1,4-diferrocenyl-1,3-butadiyne (BFc-butadiyne in Fig. 1, see SI section 1 for synthetic details), where two Fc units are electrically communicated through a butadiyne conjugated spacer. Figure 5b shows the single-molecule conductance results within the high conductance region near G_0 ($10^{-2}G_0$ to $1G_0$), which are dominated by two conductance maxima associated with the two possible bridging configurations $(BFc\text{-}butadiyne)_1$ and $(BFc\text{-}butadiyne)_2$ following the same previous notation in Figure 2. Both $(BFc\text{-}butadiyne)_n$ configurations register lower conductance values, $0.08G_0$ and $0.23\ G_0$, than the BFc counterpart, where the Fc units are directly connected by a single C-C bond. The BFc-butadiyne junction gives us the opportunity to challenge the proposed junction geometry shown in Fig. 3b as follow: we have explored a lower conductance range ($10^{-3}G_0$-$10^{-2}G_0$) to seek for possible extended configurations where the oligoFc wire is connected with the classical wiring picture through the distal Fc units[3]. To this aim, the low conductance region was analyzed for the BFc-butadiyne compound (Fig. 5a) whose side-to-side molecular conductance can be directly compare to the conductance values of the same butadiyne backbone previously measured using different anchoring chemistry.[67,68] The obtained value in 5a, $0.0034G_0$, fully agrees with previously measured conductance values of the

same compound using pyridine as the anchoring units.[67] This result constitutes a strong evidence that the conjugated spacer between the Fc units in the BFc-butadiyne dominates the charge transport in the low current range, thus reinforcing the proposed multi-contact configuration pictured in this work. This result is also captured by the transmission calculations in next section.

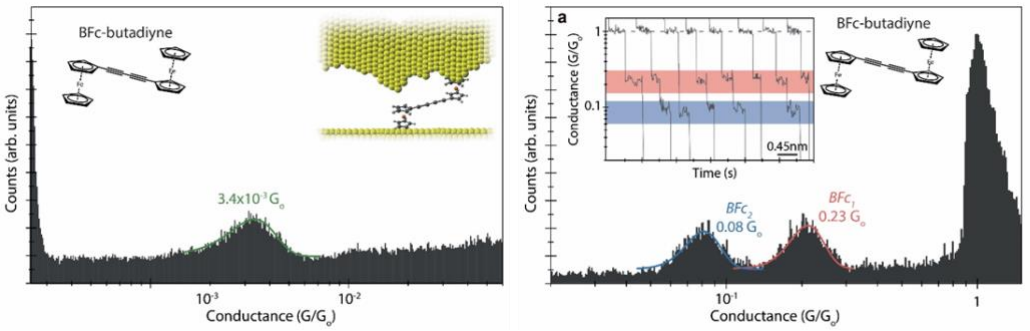

Fig. 5 Semi-log conductance histograms of BFc-butadiyne within the low range ($10^{-3}G_0$-$10^{-2}G_0$) **(a)** and high range ($10^{-2}G_0$ to $1G_0$) **(b)** of G. The conductance values are extracted from Gaussian fits of the peaks. The inset in (b) shows representative individual current traces displaying plateau features used to build the 1D histogram. The shadow colored lines indicate the range of conductance for each plateau (line width extracted from the FWHM of the fitted histogram peaks). The applied voltage bias was set to 10 mV.

DFT-orbitals and transmission functions

Table I visualizes the molecular orbitals for all studied compounds calculated using density functional theory (DFT) at the B3LYP/TZV level in the gas-phase (for details on the computational calculations see SI section 7). The HOMO levels correspond to quasi-degenerated MOs with high contributions from the metal d_{xy} and d_{x2-y2} orbitals that have a σ bonding interaction with the cyclopentadienyl (Cp) rings. A similar situation is found for the LUMO levels with the metal d_{xz} and d_{yz} orbitals that have also strong contribution of the Cp ligands with antibonding character. The computed HOMO energy (E_{HOMO}) trend along the Fc, BFc and TFc series (see Table I and SI section 7.3) correlates well with high conductance features (all connected Fc units) in the histograms of Fc, BFc_2, BFc-$butadiyne_2$ and TFc_3, and suggests the HOMO frontier orbital as the transport-relevant orbital due to its close proximity in energy to the Au Fermi energy (around -5 eV), also in agreement with previous works.[48,69–72] The correlation shows that by increasing the number of Fc units in the molecule, the E_{HOMO} level and degeneracy increase approaching the metal Fermi energy (Table I), thus decreasing the tunneling barrier height, $\delta E = E_{HOMO} - E_F$, which is in agreement with the increase in tunneling rate with increasing the oligoFc length (Fig. 3c, purple line). The DFT-computed frontier orbitals show an extended side-to-side delocalization of the HOMO in all cases (Table I). Figure 6 shows that the saturating conductance behavior going from the Fc to the all Fc connected TFc is captured by the HOMO-Fermi level alignment.

Table I. HOMO-LUMO representations of the isosurface plots (isovalue = 0.03) and energies (in eV) for the four molecular systems (see SI section 7.2 for the full MO diagrams) for all four studied compounds calculated at the B3LYP/TZV level. Adjacent energy levels (lines below the MO representation) in the same compound denote MO degeneracy, while piled up levels are energetically separated MOs. ELISEO: deberiamos poner todos los orbitales que estan cerca en energia (diferentes lineas) y poner los valores

de energía. Como afecta el tener más densidad de estados cerca del Ef ?, como entra en la transmission function?.

	HOMO		LUMO	
BFc-Butadiyne	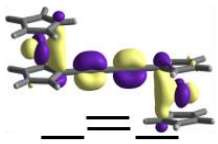	-5.40 eV	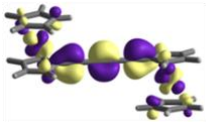	-1.36 eV
Fc	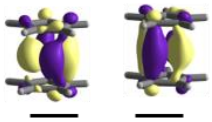	-5.44 eV	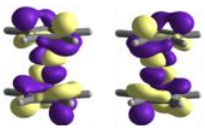	-0.488 eV
BFc	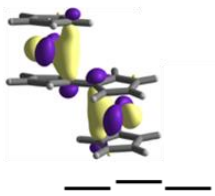	-5.28 eV	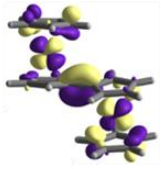	-0.742 eV
TFc	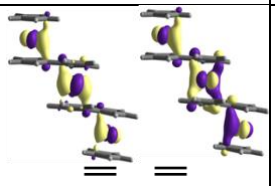	-5.25 eV	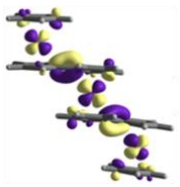	-0.833 eV

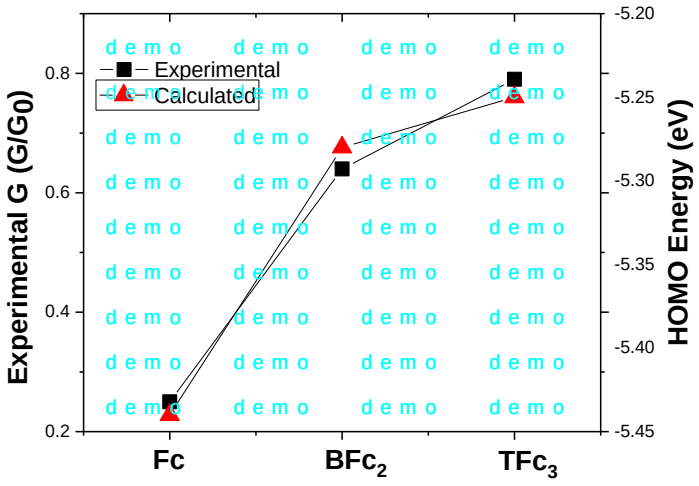

Fig. 6 Fuse this one with the corresponding cartoons of Fig. 8

We have also performed non-equilibrium Green function (NEGF) calculations combined with DFT approaches to calculate the conductance and the transmission functions (see Computational details in SI Section 7) for the three Fc, BFc, and TFc single-molecule junctions. We have employed a model structure for the junction with two gold hillocks flanking each Fc unit to simulate the STM scenario, where all Fc units are initially connected to both junction electrodes (Fig. 7a). To simulate the sequential Fc disconnection as we pull, two Au hillocks are

removed, one at a time, from one side of each two Fc units and the transmission function is recalculated for each particular case (see Fig. 7b and c, Eli, ke te parece poner solo un view, el primero, y poner los 3 casos: 3 conectados, 2 y 1). Figure 7d shows the corresponding transmission curves for the three cases (las ponemos!!). For comparison, we have also considered a more "flat" configuration where the oligoFc compound is trapped between two atomically flat surfaces (see Fig. S7.1).

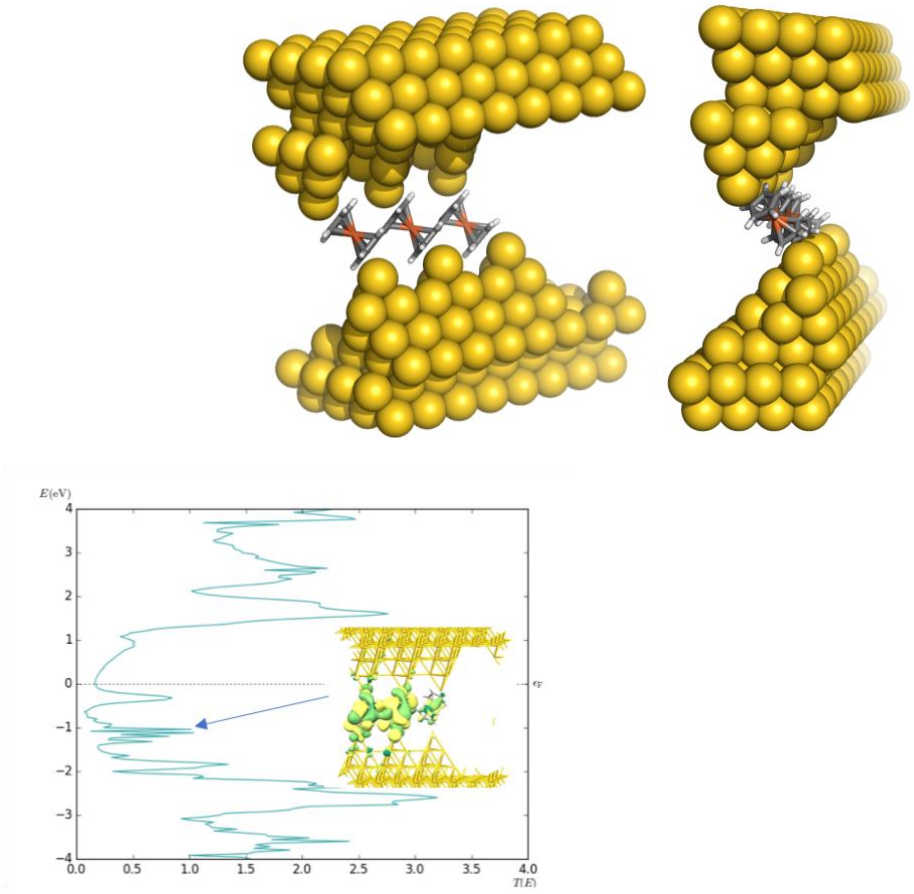

Fig. 7 Poner 1 view (left) and the three calculated case scenarios plus transmission curves de cada uno

As expected from the above orbital picture (Table I), the HOMO orbitals (d_{xy} and d_{x2-y2} combinations) contribute in all cases to the closest transmission peaks in energy below the Au Fermi level E_F, and whose tails extend all the way to the E_F (Fig. 7d). Figure 8 shows the correlation of the experimental single-molecule *G* values of the TFc compound (Figures 2c) with the integrated conductance values from the TFc transmission curves within the experimental bias windows for the cases with 1, 2 and 3 bridged Fc units (Fig. 7d). Again, the observed saturating conductance behavior (Fig. 3c, green line) is captured by the NEGF-DFT calculations.

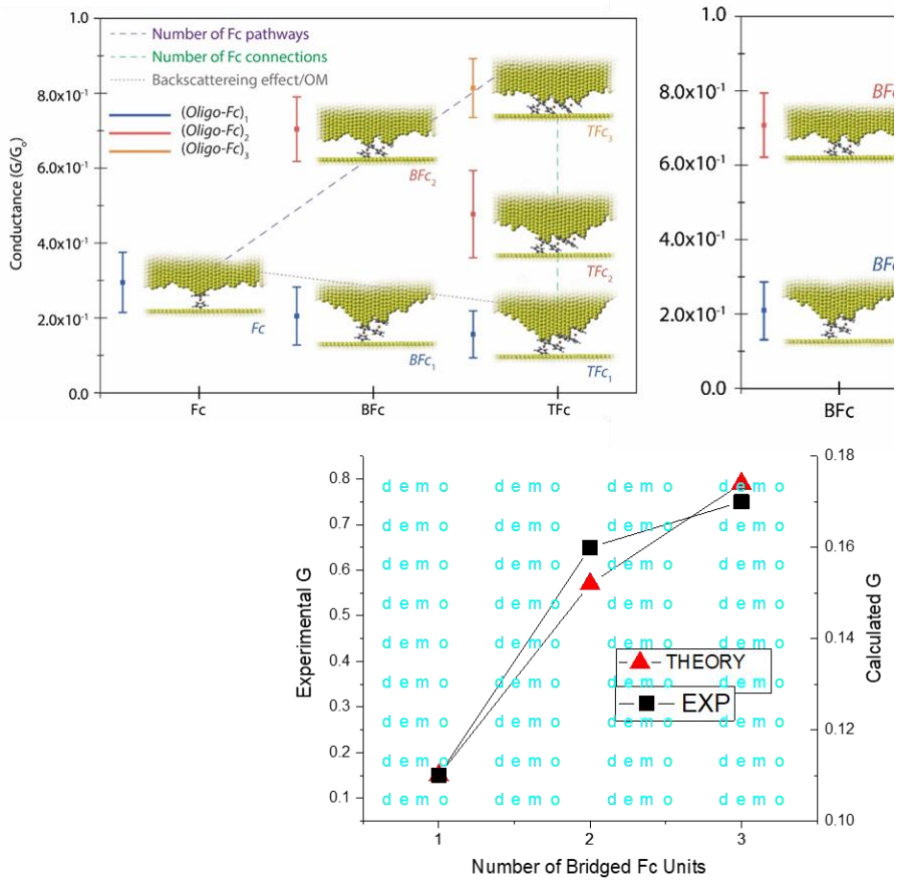

Fig. 8 (a) Fuse the upper graph with cartoons (vertical series) with the origin bottom graph.

To explain the bottom trend in Fig. 3c (grey line), we have plotted the transmission pathways for the two extreme cases: Fc and TFc_1 (Fig. 9). The direct comparison of the transmission pathways shows a better efficiency for the Fc system, as experimentally found, than for the TFc_1 case. In the latter, the lack of an effective connection through the two unbridged Fc units increases the backscattering effect in the incoming electron waves as compared to the former Fc case. (Eli, tendriamos k explicar esto mejor, yo no lo entiendo , aunque si arece claro en tu Fig. 9)

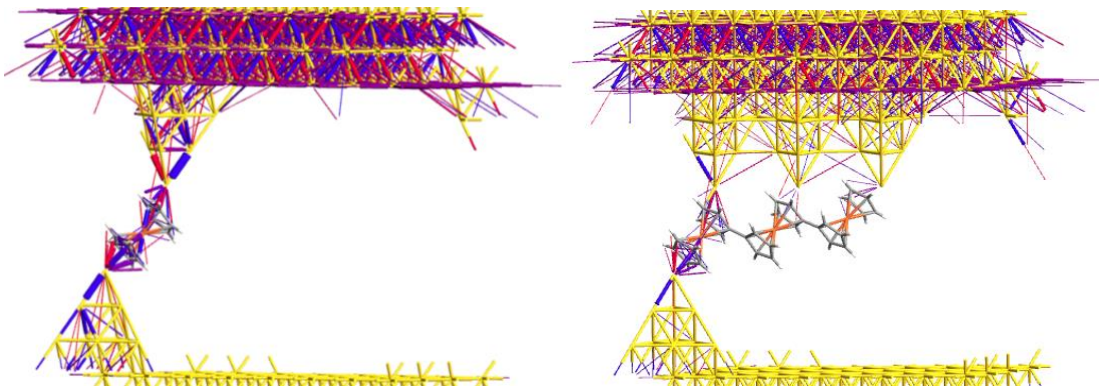

Fig. 9 Transmission pathways for the TFc models with 3+3 and 3+1 contacts and for the FC system. The color of the arrows indicates the angle of the direction of the transport, blue (0°, forwards) and red (180°, backwards), respectively and intermediate colors (0-180°). The width of the arrow is related with the magnitude of the transport.

Conclusions

In conclusion, we have measured the single-molecule conductance of a series of Fc-oligomers (Fc, BFc and TFc), which efficiently couple to two metal leads in the absence of a linker group via connecting multiple Fc units in a simultaneous fashion. The result is a highly conductive molecular wire under coherent tunneling regime, whose conductance results in exceedingly high values of up to 0.8 G_o, near the ballistic conductance quantum, G_o. Our computed DFT orbitals show that the delocalized HOMO frontier orbital increases in energy and degeneracy in the order BFc-butadiyne<Fc<BFc<TFc, approaching the Au electrode Fermi energy and explaining the same increasing conductance trend for the configurations where all Fc nits are connected. Moreover, the calculated transmission functions recreate the saturating conductance increase for each individual compound when more number of Fc units within the same backbone are being connected in the junction.

Interestingly, this work shows that the Fc units can interact strongly with the electrodes of the STM break junction most likely via the distal uncoordinated atoms at the tips of the electrodes, as opposed to other Fc-based backbones where the Fc unit is isolated by axial linkers[15,54] or SAM-based junctions with the Fc units in van der Waals contact with the electrodes[102]. The consequence is that in the former, the molecular frontier orbitals delocalize resulting in a molecular junction displaying near ballistic transport with $G=0.8G_0$, *i.e*. the junctions are in the strong coupling regime, while in the latter the molecular frontier orbital are confined in the molecule resulting in a more resistive molecular junction. These observations suggest that the design rules of these classes of junctions are very different due to differences in chemical reactivity between atomic tip-shaped and flat-like electrodes.

Overall, the results show a single-molecule wire displaying near-ballistic charge transport whose conductance can be modulated through the molecularly engineered extension of the Fc low-lying molecular orbital and the number of electrode/Fc contact points. This work also suggests the use of Fc as a new tunable molecule/electrode anchoring group with a simple contact configuration (single conductance signature) and a low energy tunneling barrier for charge injection.

Acknowledgements

This research was supported by the MINECO Spanish national projects CTQ2015-71406-ERC, CTQ2015-64579-C3-1-P and CTQ2015-64579-C3-3-P (MINECO/FEDER, EU). A.C.A. thanks the Spanish Ministerio de Educación, Cultura y Deporte for a graduate FPU fellowship. N.D. acknowledges the European Union for a Marie Curie IIF Fellowship. E. R. thanks Generalitat de Catalunya for an ICREA Academia award. I. D.-P. thanks Kings College London for startup support. The National Research Foundation (NRF) is kindly acknowledged for supporting this research under the CRP program (award No. NRF-CRP 8-2011-07). We also acknowledge the Minister of Education (MOE) for supporting this research under award No. MOE2015-T2-1-050. Prime Minister's Office, Singapore under its Medium sized centre program is also acknowledged for supporting this research.

References

1 J. C. Cuevas and E. Scheer, in *Molecular Electronics*, WORLD SCIENTIFIC, 2010, vol. 1, pp. i–xix.

2 Y. Okawa, S. K. Mandal, C. Hu, Y. Tateyama, S. Goedecker, S. Tsukamoto, T. Hasegawa, J. K. Gimzewski and M. Aono, *J. Am. Chem. Soc.*, 2011, **133**, 8227–33.

3 B. Xu and N. J. Tao, *Science*, 2003, **301**, 1221–3.

4 H. Song, Y. Kim, Y. H. Jang, H. Jeong, M. A. Reed and T. Lee, *Nature*, 2009, **462**, 1039–43.

5 I. Díez-Pérez, J. Hihath, Y. Lee, L. Yu, L. Adamska, M. a Kozhushner, I. I. Oleynik and N. Tao, *Nat. Chem.*, 2009, **1**, 635–41.

6 L. Yuan, N. Nerngchamnong, L. Cao, H. Hamoudi, E. del Barco, M. Roemer, R. K. Sriramula, D. Thompson and C. A. Nijhuis, *Nat. Commun.*, 2015, **6**, 6324.

7 A. Wan, C. S. Suchand Sangeeth, L. Wang, L. Yuan, L. Jiang and C. A. Nijhuis, *Nanoscale*, 2015, **7**, 19547–56.

8 M. Poot, E. Osorio, K. O'Neill, J. M. Thijssen, D. Vanmaekelbergh, C. A. van Walree, L. W. Jenneskens and H. S. J. van der Zant, *Nano Lett.*, 2006, **6**, 1031–1035.

9 V. B. Engelkes, J. M. Beebe and C. D. Frisbie, *J. Am. Chem. Soc.*, 2004, **126**, 14287–14296.

10 T. Hines, I. Diez-Perez, J. Hihath, H. Liu, Z. S. Wang, J. Zhao, G. Zhou, K. M??llen and N. Tao, *J. Am. Chem. Soc.*, 2010, **132**, 11658–11664.

11 E. J. Dell, B. Capozzi, J. Xia, L. Venkataraman and L. M. Campos, *Nat. Chem.*, 2015, **7**, 209–214.

12 V. Kaliginedi, P. Moreno-García, H. Valkenier, W. Hong, V. M. García-Suárez, P. Buiter, J. L. H. Otten, J. C. Hummelen, C. J. Lambert and T. Wandlowski, *J. Am. Chem. Soc.*, 2012, **134**, 5262–75.

13 I. Diez-Perez, J. Hihath, T. Hines, Z.-S. Wang, G. Zhou, K. Müllen and N. Tao, *Nat. Nanotechnol.*, 2011, **6**, 226–231.

14 R. Yamada, H. Kumazawa, T. Noutoshi, S. Tanaka and H. Tada, *Nano Lett.*, 2008, **8**, 1237–40.

15 J. S. Meisner, M. Kamenetska, M. Krikorian, M. L. Steigerwald, L. Venkataraman and C. Nuckolls, *Nano Lett.*, 2011, **11**, 1575–9.

16 B. Q. Xu, X. L. Li, X. Y. Xiao, H. Sakaguchi and N. J. Tao, *Nano Lett.*, 2005, **5**, 1491–1495.

17 L. Venkataraman, Y. S. Park, A. C. Whalley, C. Nuckolls, M. S. Hybertsen and M. L. Steigerwald, *Nano Lett.*, 2007, **7**, 502–6.

18 A. C. Aragonès, N. Darwish, J. Im, B. Lim, J. Choi, S. Koo and I. Díez-Pérez, *Chem. - A Eur. J. (Weinheim an der Bergstrasse, Ger.*, 2015, **21**, 7716–20.

19 X. Xiao, L. A. Nagahara, A. M. Rawlett and N. Tao, *J. Am. Chem. Soc.*, 2005, **127**, 9235–9240.

20 W. Haiss, H. van Zalinge, D. Bethell, J. Ulstrup, D. J. Schiffrin and R. J. Nichols, *Faraday Discuss.*, 2006, **131**, 253–264.

21 L. Venkataraman, J. E. Klare, C. Nuckolls, M. S. Hybertsen and M. L. Steigerwald, *Nature*, 2006, **442**, 904–7.

22 D. Vonlanthen, A. Mishchenko, M. Elbing, M. Neuburger, T. Wandlowski and M. Mayor, *Angew. Chemie Int. Ed.*, 2009, **48**, 8886–8890.

23 F. Chen and N. J. Tao, *Acc. Chem. Res.*, 2009, **42**, 429–38.

24 * C. D. Zangmeister, S. W. Robey, † and R. D. van Zee, J. G. Kushmerick, J. Naciri, Y. Y. and, J. M. Tour, B. Varughese, and B. Xu and J. E. Reutt-Robey, , DOI:10.1021/JP060228U.

25 L. Yuan, C. Franco, N. Crivillers, M. Mas-Torrent, L. Cao, C. S. S. Sangeeth, C. Rovira, J. Veciana and C. A. Nijhuis, *Nat. Commun.*, 2016, **7**, 12066.

26 B. Kim, J. M. Beebe, Y. Jun, X.-Y. Zhu and C. D. Frisbie, *J. Am. Chem. Soc.*, 2006, **128**, 4970–4971.

27 W. Chen, H. Li, J. R. Widawsky, C. Appayee, L. Venkataraman and R. Breslow, *J. Am. Chem. Soc.*, 2014, **136**, 918–20.

28 F. Chen, X. Li, J. Hihath, Z. Huang and N. Tao, *J. Am. Chem. Soc.*, 2006, **128**, 15874–15881.

29 Y. S. Park, A. C. Whalley, M. Kamenetska, M. L. Steigerwald, M. S. Hybertsen, C. Nuckolls and L. Venkataraman, *J. Am. Chem. Soc.*, 2007, **129**, 15768–9.

30 W. Hong, D. Z. Manrique, P. Moreno-García, M. Gulcur, A. Mishchenko, C. J. Lambert, M. R. Bryce and T. Wandlowski, *J. Am. Chem. Soc.*, 2012, **134**, 2292–304.

31 L. A. Zotti, T. Kirchner, J.-C. Cuevas, F. Pauly, T. Huhn, E. Scheer and A. Erbe, *Small*, 2010, **6**, 1529–1535.

32 T. J. KEALY and P. L. PAUSON, *Nature*, 1951, **168**, 1039–1040.

33 R. F. Dou, D. Y. Zhong, W. C. Wang, K. Wedeking, G. Erker, L. Chi and H. Fuchs, *J. Phys. Chem. C*, 2007, **111**, 12139–12144.

34 L. Yuan, R. Breuer, L. Jiang, M. Schmittel and C. A. Nijhuis, *Nano Lett.*, 2015, **15**, 5506–12.

35 C. Waldfried, D. Welipitiya, C. W. Hutchings, H. S. V. de Silva, G. A. Gallup, P. A. Dowben, W. W. Pai, J. Zhang, J. F. Wendelken and N. M. Boag, *J. Phys. Chem. B*, 1997, **101**, 9782–9789.

36 B. W. Heinrich, L. Limot, M. V Rastei, C. Iacovita, J. P. Bucher, D. M. Djimbi, C. Massobrio and M. Boero, *Phys. Rev. Lett.*, 2011, **107**, 216801.

37 C. Morari, I. Rungger, A. R. Rocha, S. Sanvito, S. Melinte and G.-M. Rignanese, *ACS Nano*, 2009, **3**, 4137–4143.

38 P. . Dowben, C. Waldfried, T. Komesu, D. Welipitiya, T. McAvoy and E. Vescovo, *Chem. Phys. Lett.*, 1998, **283**, 44–50.

39 R. C. Quardokus, N. A. Wasio, R. P. Forrest, C. S. Lent, S. A. Corcelli, J. A. Christie, K. W. Henderson and S. A. Kandel, *Phys. Chem. Chem. Phys.*, 2013, **15**, 6973–81.

40 M. Ormaza, P. Abufager, N. Bachellier, R. Robles, M. Verot, T. Le Bahers, M.-L. Bocquet, N. Lorente and L. Limot, *J. Phys. Chem. Lett.*, 2015, **6**, 395–400.

41 D. Welipitiya, P. A. Dowben, J. Zhang, W. W. Pai and J. F. Wendelken, *Surf. Sci.*, 1996, **367**, 20–32.

42 C. M. Woodbridge, D. L. Pugmire, R. C. Johnson, N. M. Boag and M. A. Langell, *J. Phys. Chem. B*, 2000, **104**, 3085–3093.

43 X. Xiao, D. Brune, J. He, S. Lindsay, C. B. Gorman and N. Tao, *Chem. Phys.*, 2006, **326**, 138–143.

44 S. Getty, C. Engtrakul, L. Wang, R. Liu, S.-H. Ke, H. Baranger, W. Yang, M. Fuhrer and L. Sita, *Phys. Rev. B*, 2005, **71**, 241401.

45 Q. Lu, C. Yao, X. Wang and F. Wang, *J. Phys. Chem. C*, 2012, **116**, 17853–17861.

46 Y.-Y. Sun, Z.-L. Peng, R. Hou, J.-H. Liang, J.-F. Zheng, X.-Y. Zhou, X.-S. Zhou, S. Jin, Z.-J. Niu and B.-W. Mao, *Phys. Chem. Chem. Phys. Phys. Chem. Chem. Phys*, 2260, **16**, 2260–2267.

47 J. He and S. M. Lindsay, *J. Am. Chem. Soc.*, 2005, **127**, 11932–3.

48 C. A. Nijhuis, W. F. Reus and G. M. Whitesides, *J. Am. Chem. Soc.*, 2010, **132**, 18386–401.

49 O. Gidron, Y. Diskin-Posner and M. Bendikov, *Chemistry*, 2013, **19**, 13140–50.

50 P. Aguirre-Etcheverry and D. O'Hare, *Chem. Rev.*, 2010, **110**, 4839–64.

51 G. Leatherman, E. N. Durantini, D. Gust, T. A. Moore, A. L. Moore, S. Stone, Z. Zhou, P. Rez, Y. Z. Liu and S. M. Lindsay, *J. Phys. Chem. B*, 1999, **103**, 4006–4010.

52 M. Iwane, S. Fujii, T. Nishino and M. Kiguchi, *J. Phys. Chem. C*, 2016, acs.jpcc.5b12728.

53 D. Miguel, L. Álvarez de Cienfuegos, A. Martín-Lasanta, S. P. Morcillo, L. A. Zotti, E. Leary, M. Bürkle, Y. Asai, R. Jurado, D. J. Cárdenas, G. Rubio-Bollinger, N. Agraït, J. M. Cuerva and M. T. González, *J. Am. Chem. Soc.*, 2015, **137**, 13818–13826.

54 M. S. Inkpen, M. Lemmer, N. Fitzpatrick, D. C. Milan, R. J. Nichols, N. J. Long and T. Albrecht, *J. Am. Chem. Soc.*, 2015, **137**, 9971–9981.

55 T. Hines, I. Díez-Pérez, H. Nakamura, T. Shimazaki, Y. Asai and N. Tao, *J. Am. Chem. Soc.*, 2013, **135**, 3319–22.

56 A. C. A. C. Aragonès, D. Aravena, J. I. J. I. Cerdá, Z. Acís-Castillo, H. Li, J. A. J. A. Real, F. Sanz, J. Hihath, E. Ruiz and I. Díez-Pérez, *Nano Lett.*, 2016, **16**, 218–226.

57 S. Afsari, Z. Li and E. Borguet, *Angew. Chemie Int. Ed.*, 2014, **53**, 9771–9774.

58 K.-H. Müller, *Phys. Rev. B*, 2006, **73**, 45403.

59 K. Ishizuka, M. Suzuki, S. Fujii, Y. Takayama, F. Sato and M. Fujihira, *Jpn. J. Appl. Phys.*, 2006, **45**, 2037–2040.

60 C. Li, I. Pobelov, T. Wandlowski, A. Bagrets, A. Arnold and F. Evers, *J. Am. Chem. Soc.*, 2008, **130**, 318–326.

61 X. Li, J. He, J. Hihath, B. Xu, S. M. Lindsay and N. Tao, *J. Am. Chem. Soc.*, 2006, **128**, 2135–2141.

62 P. Moreno-García, A. La Rosa, V. Kolivoška, D. Bermejo, W. Hong, K. Yoshida, M. Baghernejad, S. Filippone, P. Broekmann, T. Wandlowski and N. Martín, *J. Am. Chem. Soc.*, 2015, **137**, 2318–27.

63 M. Kiguchi, T. Ohto, S. Fujii, K. Sugiyasu, S. Nakajima, M. Takeuchi and H. Nakamura, *J. Am. Chem. Soc.*, 2014, **136**, 7327–7332.

64 A. Mishchenko, L. A. Zotti, D. Vonlanthen, M. Bürkle, F. Pauly, J. C. Cuevas, M. Mayor and T. Wandlowski, *J. Am. Chem. Soc.*, 2011, **133**, 184–187.

65 P. Makk, D. Tomaszewski, J. Martinek, Z. Balogh, S. Csonka, M. Wawrzyniak, M. Frei, L. Venkataraman and A. Halbritter, *ACS Nano*, 2012, **6**, 3411–23.

66 S. T. Schneebeli, M. Kamenetska, Z. Cheng, R. Skouta, R. a. Friesner, L. Venkataraman and R. Breslow, *J. Am. Chem. Soc.*, 2011, **133**, 2136–2139.

67 C. Wang, A. S. Batsanov, M. R. Bryce, S. Martín, R. J. Nichols, S. J. Higgins, V. M. García-Suá Rez and C. J. Lambert, , DOI:10.1021/ja9061129.

68 D. Costa Milan, O. A. Al-Owaedi, M.-C. Oerthel, S. Marqués-González, R. J. Brooke, M. R. Bryce, P. Cea, J. Ferrer, S. J. Higgins, C. J. Lambert, P. J. Low, D. Z. Manrique, S. Martin, R. J. Nichols, W. Schwarzacher and V. M. García-Suárez, *J. Phys. Chem. C*, 2015, acs.jpcc.5b08877.

69 F. C. D. A. Lima, A. Calzolari, M. J. Caldas, R. M. Iost, F. N. Crespilho and H. M. Petrilli, *J. Phys. Chem. C*, 2014, **118**, 23111–23116.

70 S. U. Lee, R. V. Belosludov, H. Mizuseki and Y. Kawazoe, *J. Phys. Chem. C*, 2007, **111**, 15397–15403.

71 T. Bredow, C. Tegenkamp, H. Pfnür, J. Meyer, V. V Maslyuk and I. Mertig, *J. Chem. Phys.*, 2008, **128**, 64704.

72 H. Jeong, D. Kim, G. Wang, S. Park, H. Lee, K. Cho, W.-T. Hwang, M.-H. Yoon, Y. H. Jang, H. Song, D. Xiang and T. Lee, *Adv. Funct. Mater.*, 2014, **24**, 2472–2480.